



## OPEN ACCESS

## EDITED BY

Surender Kumar Sharma,  
Federal University of Maranhão, Brazil

## REVIEWED BY

Jose Martin Yañez Limon,  
National Polytechnic Institute, Mexico  
Lipeng Xin,  
Xi'an Jiaotong University, China

## \*CORRESPONDENCE

Dr. Rashi Nathawat,  
✉ rashi.nathawat@gmail.com

## SPECIALTY SECTION

This article was submitted to Condensed Matter Physics, a section of the journal Frontiers in Physics

RECEIVED 19 December 2022

ACCEPTED 23 January 2023

PUBLISHED 24 February 2023

## CITATION

Sharma VK, Kumawat AK, Rathore SS, Sulania I, Meena RC, Kedia SK and Nathawat DR (2023), The SHI irradiation induced transition to negative dielectric constant phase in  $K_2Bi_4Ti_4WO_{18}$ . *Front. Phys.* 11:1127118. doi: 10.3389/fphy.2023.1127118

## COPYRIGHT

© 2023 Sharma, Kumawat, Rathore, Sulania, Meena, Kedia and Nathawat. This is an open-access article distributed under the terms of the [Creative Commons Attribution License \(CC BY\)](https://creativecommons.org/licenses/by/4.0/). The use, distribution or reproduction in other forums is permitted, provided the original author(s) and the copyright owner(s) are credited and that the original publication in this journal is cited, in accordance with accepted academic practice. No use, distribution or reproduction is permitted which does not comply with these terms.

# The SHI irradiation induced transition to negative dielectric constant phase in $K_2Bi_4Ti_4WO_{18}$

Vipul K. Sharma<sup>1</sup>, Ashish K. Kumawat<sup>1</sup>, Satyapal S. Rathore<sup>2</sup>,  
Indra Sulania<sup>3</sup>, R. C. Meena<sup>3</sup>, S. K. Kedia<sup>3</sup> and Dr. Rashi Nathawat<sup>1\*</sup>

<sup>1</sup>Functional Ceramics and Smart Materials Lab, Department of Physics, Manipal University Jaipur, Jaipur, India,

<sup>2</sup>Department of Physics, Cluster University of Jammu, Jammu, India, <sup>3</sup>Inter-University Accelerator Centre, New Delhi, India

In present communication, a new Aurivillius family compound  $K_2Bi_4Ti_4WO_{18}$  was synthesized, and the impact of swift heavy ion (SHI),  $Ni^{+11}$  irradiation on its surface and dielectric properties has been studied in detail. The phase formation in this complex oxide, and crystallization to  $B2cb$  symmetry was confirmed by the X-ray diffraction. However, post irradiation the XRD, SEM and AFM studies shows the surface amorphization, in agreement with the theoretical calculations. Furthermore, the effect of irradiation was also observed in the bulk dielectric properties as the system transform to a phase with negative dielectric constant above 350 K in the radio frequencies. This transition is in correlation with significant change in other dielectric parameters such enhancement in AC conductivity, a helical Nyquist plot and multiple dielectric relaxations. This conspicuous changes in the dielectric response post irradiation is attributed to the SHI induced defect formation, modification of energy barriers and their consequences on the electronic structure. Thus, current study suggests that the dielectric properties of Aurivillius  $K_2Bi_4Ti_4WO_{18}$  could be tailored by ion irradiation and opens a new possibility of tuning functional properties.

## KEYWORDS

swift heavy ion irradiation, impedance spectroscopy, phase transition, aurivillius ceramic oxides, negative index

## 1 Introduction

The electric permittivity  $\epsilon$ , and the magnetic permeability  $\mu$ , are the fundamental quantities which determine the interaction of electromagnetic waves with matter [1–3]. These indices also dictate many physical and optical properties of materials. Depending on  $\epsilon$  and  $\mu$ , the field-matter interaction induces magnetization and polarization in magnetic materials and dielectric materials respectively. Both polarization and magnetization also produce their own fields, and the interaction of these fields with the external fields, result in a large spectrum of dielectric and magnetic phenomena. In the present work we'll limit our discussion to dielectric systems, which is equally applicable to magnetic systems due to the correlation as derived by Maxwell's equations [4, 5]. The dielectric constant for a linear, homogeneous and isotropic dielectric medium is given by  $\epsilon_r = 1 + \chi$ , where  $\chi$  is electric susceptibility. This  $\chi$  is further related to the polarization,  $\mathbf{P} = (\epsilon_0)\chi\mathbf{E}$ , where  $\epsilon_0$  is permittivity of free space and  $\mathbf{E}$ , is the electric field intensity; indicating a dependence of dielectric constant on polarization. These macroscopic properties ( $\epsilon_r$ ,  $P$ ) in a non-polar dielectric are linked to the microscopic quantity (polarizability) by the famous Clausius-Mossotti relation  $\frac{(\epsilon_r-1)}{(\epsilon_r+1)} = \frac{N\alpha}{3\epsilon_0}$ , where  $N$  is the number of atoms/molecules per unit mole and  $\alpha$  is polarizability. As the  $N\alpha/(3\epsilon_0)$  approaches unity  $\epsilon_r$  approaches infinity and above critical value of density the  $\epsilon_r$  tends to be negative, popularly known as Clausius-Mossotti catastrophe. The possibility of such a system having a rare combination of negative indices  $\epsilon < 0$

and  $\mu < 0$  was proposed more than 50 years ago by Veselago in 1968 [6]. These “negative index meta-materials” if envisaged will have broad range of non-intuitive properties and applications such as superlenses, inverse Doppler effect, reverse Cherenkov radiation, anomalous refraction, optical tunneling devices and many novel devices, which may overcome the current limitations in positive index systems.

This idea, although allowed by fundamental electrodynamics principles, remain obscure for more than 30 years as it was not observed in any natural material. Based on the idea of a split ring resonator proposed by [7, 8] were able to experimentally demonstrate the idea of negative indexed systems. The composite system with a periodic array of interspaced conducting non-magnetic split ring resonators and continuous wires exhibits negative effective permittivity and permeability at microwave frequencies. In the recent past many such ‘composite’ systems were devised to show the negative indices. The systems with either of indices negative at a certain frequency, although rare, are also reported and do not violate the fundamental physical laws [9, 10]. Thus, materials with negative index ( $\epsilon < 0$ ,  $\mu < 0$ ) are of considerable scientific interest due to rich physical phenomena and large possibilities of novel photonic and electronic devices.

In present work a comparative study of Aurivillius  $K_2Bi_4Ti_4WO_{18}$ , before and after  $Ni^{+11}$  irradiation is reported in detail. The Aurivillius family compounds have attracted a flurry of research activities in the last few decades. These complex oxides possesses excellent dielectric and ferroelectric properties even at high temperatures and thus have many potential applications such as high-temperature actuators, sensors, energy harvesters, multi-layered ceramic capacitors, etc [11–17]. The Aurivillius family also known as bismuth layered ferroelectrics (BLFs) is represented by  $[Bi_2O_2]^{2+} [A_{m-1}B_mO_{3m+1}]^{2-}$ . Here A is mono, di, or trivalent element or their mixture, B is tetravalent, pentavalent element or their mixture. The value of  $m = 1, 2, 3, 4$  or 5 represent the number of perovskite like units of  $ATiO_3$  sandwiched between  $Bi_2O_2$  layers. Due to a large possible combination of A and B sites as well as m, many derivatives of BLFs have been reported in the literature [18,19]. These materials can be a good substitute in the search for environmentally friendly lead-free electro-ceramics [20, 21]. Furthermore, their dielectric response can be tuned by partial or complete A, B, and Bi site substitutions. In addition, a careful control of synthesis conditions and processing parameters was also reported to be effective in controlling their functional properties. Another approach to tailor the bulk dielectric properties is by surface modification of these complex oxides [18]; [22, 23]. The ion implantation, which is based on ion-matter interaction, is a reliable technique to modify the materials property [24, 25]. Depending on the type of interaction, the ion implantation can be used for modification of a wide class of materials: metals, dielectrics, polymers, ceramics, alloys and composites [26–34]. The swift heavy-ion (SHI) irradiation is its subset which explores the interaction of ions with mass equal or greater than Carbon and energies MeV/amu. The SHI typically produces a controlled track of damage in an insulator. Depending on the interaction a wide range of radiation defects: point defects, vacancies, amorphization, defect cluster, imperfections, and lattice strain were reported [35–38]. Previous reports have demonstrated that SHI implantation by controlling irradiation parameters is capable of inducing far-from-equilibrium material properties and phases [39, 40]. This article reports the effects of heavy ion irradiation on the dielectric response of the Aurivillius

family  $K_2Bi_4Ti_4WO_{18}$ . This SHI induced surface amorphization was observed to induce a transition to a negative indexed phase above room temperature in radio frequencies.

## 2 Experimental section

For synthesis of polycrystalline  $K_2Bi_4Ti_4WO_{18}$  (KBTW) solid-state reaction technique was employed. The stoichiometric amount of high purity (Sigma-Aldrich)  $K_2CO_3$ ,  $Bi_2O_3$ ,  $TiO_2$ , and  $WO_6$  were taken as precursors. The powder mixture was mixed well using mortar and pestle and then ball milled for 6 h, followed by intermediate calcination at 950°C for 8 h. The calcined powder mixed with PVA binder was then pressed into a pellet (12 mm dia, and 1 mm thick), in a uni-axial press. The pellets were then sintered at 1,100 for 2 hours. These pellets were uniformly exposed to  $Ni^{+11}$  of 150 MeV energy at fluence of  $5 \times 10^{12}$  ions/cm<sup>2</sup>. The SHI irradiation was carried out at UD Pelletron Accelerator at Inter University Accelerator Centre (IUAC), New Delhi. The room temperature XRD measurement of pristine (unirradiated) and irradiated samples was performed using BRUKER D-8 X-ray diffractometer with  $Cu - K\alpha$  radiation of 1.54 Å. The SEM imaging was performed with a JEOL make JSM-7610F Plus FESEM. The AFM was performed using Veeco Instruments Inc. made a Multi-Mode SPM system with a Nanoscope IIIa controller. The temperature (100K–420K) dependent dielectric measurement was performed using an Agilent LCR meter in a frequency range of 10Hz–2 MHz. (Model No E4980A) with Lakeshore temperature controller (Model no-340). The initial calculation of expected radiation damage was performed using Stopping and Range of Ions in Matter (SRIM) software.

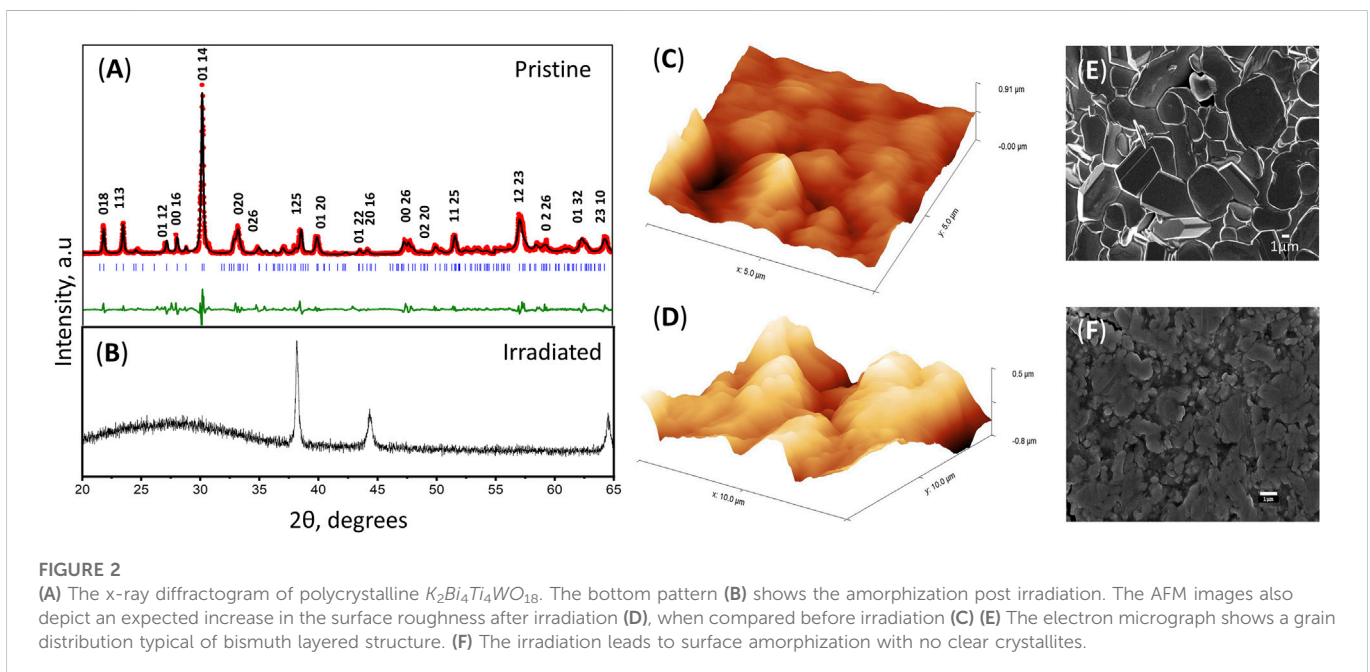
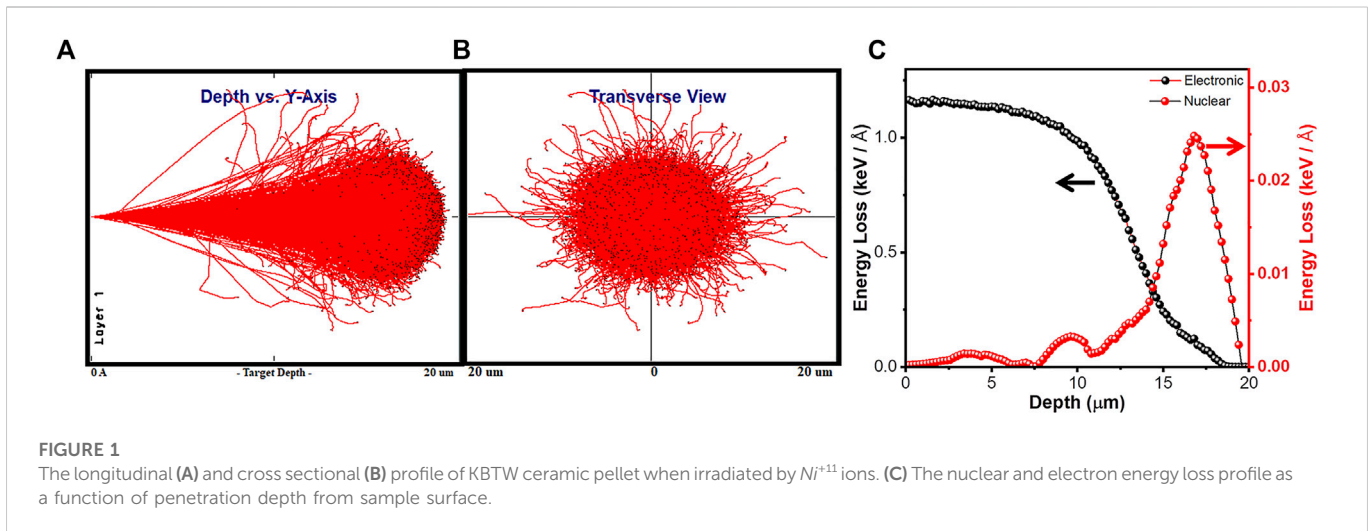
### 2.1 Stopping and range of ions in matter (SRIM) simulation

The depth profile of 150 MeV  $Ni^{+11}$  ions in KBTW crystal was theoretically simulated by SRIM software [41]. Figures 1A, B shows the longitudinal and cross-sectional view respectively post normal irradiation which suggests a nearly homogeneous irradiation effect. The energetic ions while penetrating predominantly loses its energy either *via* collision with nuclei (Sn) or with the atomic electrons (Se). The energy loss by these two processes in KBTW is summarized in Figure 1C. It is evident that the inelastic interaction with electron (Se) dominates initially upto a depth of 12 μm with a initial maximum value of 1.2 keV/Å. Thereafter, the nuclear interactions start increasing with a maximum at 0.025 keV/Å for penetration depth of 18 μm. Thus, based on thermal spike model the top layer from surface up to 12 μm can be considered as electron loss layer and from 12 μm to 19 μm as nuclear loss layer. Thus the type of defects and imperfections created by ion track will vary from surface to penetration 17 μm with a straggle of 15 μm.

## 3 Results and discussion

### 3.1 Structural and surface studies

The Le-Bail analysis of the pristine sample is represented in Figure 2A. As evident from the Le-Bail fitting, all the observed peaks belongs to the orthorhombic  $B2cb$  space group-symmetry

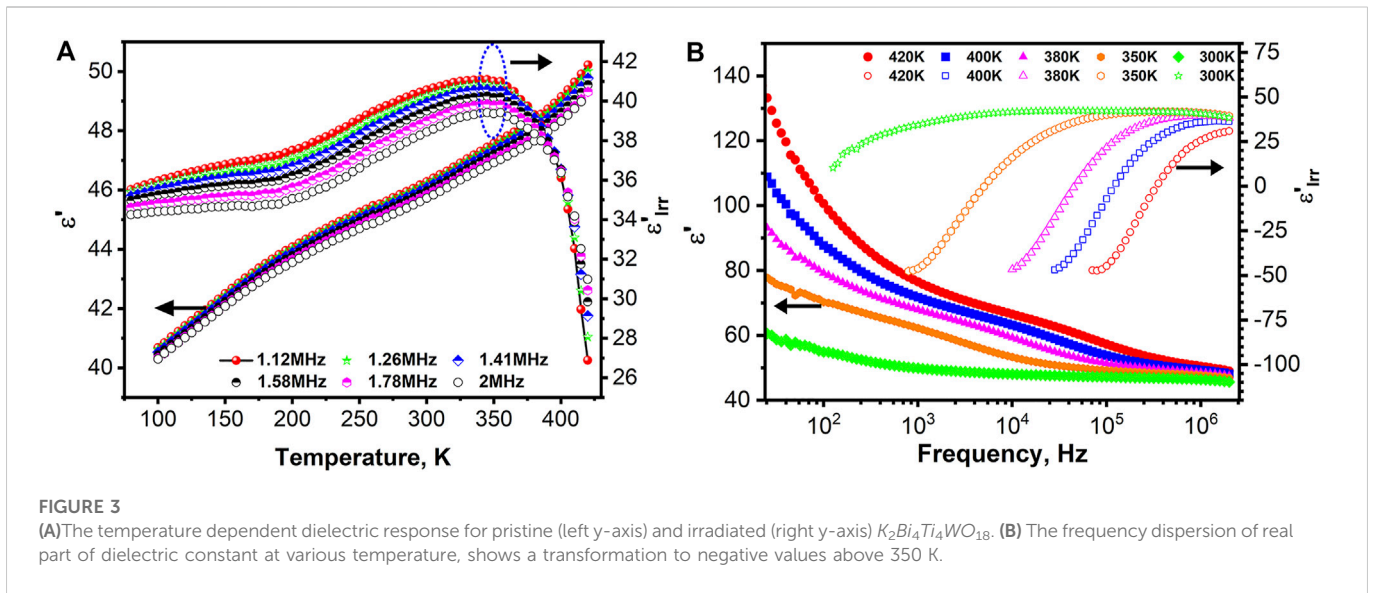


with  $a = 5.6085(12)$ ,  $b = 5.38146$ , and  $c = 49.4763$  Å, respectively. The structure parameters clearly indicate that crystal structure of KBTW is similar to a typical Aurivillius structures with 5-layered perovskite stacking sandwich between  $Bi_2O_2$  layers. A detailed structural analysis is in communication and hence not discussed in this article. The penetration of ions ( $20\ \mu m$ ) is much larger than the interaction depth of x-rays in solids and thus explains the observed amorphous nature in irradiated ceramic (Figure 2B, bottom curve). This result is agreement with the SRIM calculations [42, 43].

The tapping mode AFM imaging was carried out to examine the surface effects and is shown in Figures 2C, D for pristine and irradiated sample respectively. The roughness profile for both the samples was measured with the aid of inbuilt processing software. The root mean square roughness of the sample shows nearly 10 times increase post treatment. The sample also shows formation of deep trenches, cracks

and grain damage. A visible change is colour towards dark shade can be understood by localized heating caused while losing of ion energy to the lattice. This result is consistent with other published works in functional ceramics [44-46].

To characterize the microstructural changes, the secondary electron imaging was performed. The unirradiated KBTW ceramic shows a plate like grain morphology, typical of bismuth layered structures Figure 2E. The grain distribution in sintered sample has an average crystallite size of  $0.36\ \mu m$ . The changes induced by  $Ni^{+11}$  ions in its irradiated counterpart is clearly visible in electron micrograph, Figure 2F. The crystallites are fragmented into smaller grains and the agglomeration to form clusters is also observed. Due to diffused grain boundaries, it is challenging to measure the grain size after irradiation. This irradiation damage can be understood by the distribution of kinetic energy of the ions to the lattice. If the energy



imparted is greater than the binding energy, the excessive energy can rise the local temperature resulting in localize melting, resulting in the observed amorphization of the surface [47, 48]. A more information on defect kinetics and grain dynamics during ion-beam exposure, can be gained by *in situ* measurements [49]. Thus, the combination of XRD, AFM and SEM provides more comprehensive information of surface morphology, and internal damage structure.

### 3.2 Broadband dielectric study

The temperature (100K–420 K) and frequency (10 Hz–2 MHz) dependence of the real part of the dielectric constant ( $\epsilon'$ ) for KBTW ceramics before and after irradiation is shown in Figure 3. The  $\epsilon'$  was observed to show a low frequency dispersion for KBTW with large values at low frequency (Figure 3B) and decrease monotonically with increase in frequency. The pristine KBTW follows a non-linear modified Debye equation. This equation indicate the presence of multiple relaxation mechanism due to surface boundaries effects, usually dominating at lower frequencies, and also termed Maxwell-Wagner (MW) polarization [5]; [50–52]. The  $\epsilon'$  was also observed to show a temperature dependence, and increases with temperature. However, no dielectric phase transition was observed for the pristine KBTW in the performed experimental range of temperature. This frequency and temperature dependence is in agreement with conventional dielectric systems [53–55]. As mentioned in the introduction the dielectric constant is related to the total polarizability by Clausius-Mossotti relation. Different polarization mechanisms such electronic, ionic, orientational, space charge and hopping creates dipoles and add to give total polarizability of the system [5]. The dielectric behavior for irradiated sample can be divided into two parts below and above 350 K. Below the transition temperature, the dielectric constant was observed to show an appreciable decrease in dielectric constant. A comparative change post irradiation at high frequency (2 MHz) is summarized in Table 1. This decrease in dielectric constant is attributed to the introduction of defects by irradiation which provides additional inertia to dipole relaxations.

**TABLE 1** The comparative dielectric values for pre- and post-irradiated samples at discrete temperatures and a fix frequency of 2 MHz.

Temperature, K	$\epsilon'$	Irr $\epsilon'$	% Change
100	40.29	34.41	14.59
150	42.07	34.64	17.66
200	43.55	35.05	19.55
250	44.69	36.6	18.12
300	45.72	38.44	15.92
350	46.91	39.36	16.09

Notably, the irradiated sample shows an anomalous change with increase in temperature near 350 K indicating a phase transition. This drop in dielectric constant (Irr  $\epsilon'$ ) was observed to show a frequency dependence as well. Interestingly, in irradiated KBTW the dielectric constant further drops to negative value above critical temperature (350 K) at radio frequencies. This anomalous transformation to negative dielectric constant state *via* SHI irradiation is not reported in literature. In presence of an external electric excitation all the conventional polarization mechanisms (electronic, ionic, orientational, hopping, space charge and spontaneous) aligns in the direction of field. All the induced as well as preexisting dipoles add up to give a positive value of effective dielectric constant. The negative value suggests that the net polarization opposes the external field. In present case the transition was observed above TC, indicating the thermally activated mechanism. This could be understood as either increase in the value of depolarizing.

Field (which opposes the applied field) or creation of new dipolar mechanism induced by SHI plausibly by trapping of charge carriers. A similar response was observed in polycrystalline  $PrMnO_3$ , wherein negative value is explained by modified Drude model which allows the formation of electron-electron pair [56].

**Modulus Study:** The frequency dependence of imaginary part of the modulus for temperatures above transition temperature shows frequency dependence (Figure 4A). The broad dispersive peak representing a dielectric relaxation is shown by solid symbols for

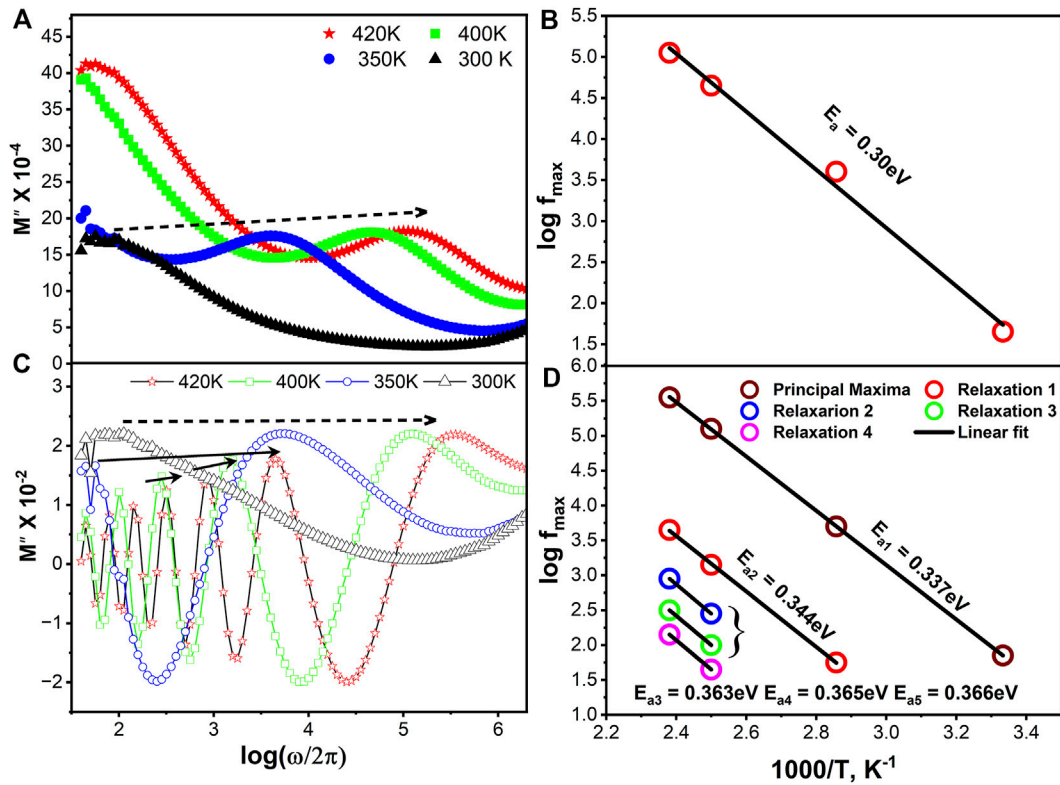


**FIGURE 4** The frequency dispersion of imaginary part of modulus at discrete temperatures for pristine (A) (shown by solid symbols) and irradiated (C) (shown by hollow symbols)  $K_2Bi_4Ti_4WO_{18}$ . The activation energy profile for pristine (B) and irradiated (D) KBTW shows activation energies corresponding to different relaxations.

pristine  $K_2Bi_4Ti_4WO_{18}$ . The peak maxima ( $\omega_{max}$ ) shift towards higher frequency with increase in temperature showing presence of a glassy phase. The irradiated ceramic also exhibit a similar dispersive peak with higher value of  $M''$  and a small change in  $\omega_{max}$ . Surprisingly, in addition to a broad dispersive peak several dispersive peaks were observed (Figure 4B). The irradiated ceramic also exhibit a similar dispersive peak with higher value of  $M''$  and a small change in  $\omega_{max}$ . Surprisingly, in addition to a broad dispersive peak several dispersive peaks were observed. The temperature dependence of frequency maximum ( $\omega_{max}$ ) follows an Arrhenius relaxation given by  $\omega_{max} = Ae^{(-E_a/K_B T)}$  where  $E_a$  is activation energy,  $K_B$  is Boltzmann's constant and T is temperature. A single activation barrier in pristine sample is found at 0.3 eV, while that for irradiated sample is at 0.337 eV. The higher activation energy is in agreement with decrease in value of dielectric constant. Notably, the irradiated sample shows multiple relaxation maxima's with different barrier height. Thus the potential profile of irradiated samples can be seen as a system with multiple activation energies. As a result different relaxation mechanisms will dominate depending on the signal frequency, and temperature. At high temperature mechanism with high activation energy dominates whereas on decreasing temperature lower barrier hopping will become more probable. These temperature and frequency dependent peak maxima's shows the presence of multiple dielectric relaxations, which are induced by Ni+11 ion implantation. A similar relaxation is observed in relaxor ferroelectrics, wherein the presence of short range polar nano regions have been known to shows a second order dispersive phase transition to ordered state. It is possible for SHI's to create defects

and local electric order by displacing ions from their equilibrium positions. This isolated short range orders are plausible reason for observed multiple 'glass-like' dielectric dispersion [57, 58].

**AC Conductivity Study:** The frequency dependence of the real part of the ac conductivity,  $\sigma'$  at different temperatures above transition temperature is shown in Figure 5A. The conductivity was observed to increase with temperature, indicating a thermally activated charge transport in these ceramic. However, a significant enhancement (7 times) in conductivity was also observed post irradiation. This SHI induced enhancement can be understood by introduction of charge carriers by metallic Ni+11 ions. These values are in agreement with the dielectric response. However, no anomalous change in the conductivity (which is related to  $\epsilon''$ ) above the transition temperature suggest the dielectric response is intrinsic in nature. The real part of the ac conductivity,  $\sigma'$  was observed to follow the universal response proposed by Jonscher:  $\sigma(\omega, T) = \sigma_{dc} + A\omega^n$ , where  $\omega$  is angular frequency, T is temperature,  $\sigma_{dc}$  is dc conductivity, and A is a constant, and n is a temperature dependent exponent [59]. A deviation from this 'universal' response can be seen in the (inset of 5 A)) irradiated samples. The energy imparted by SHI's is extremely large and can cause disruption in terms of breaking of bonds, introduction of defects, strain and vacancies. This result in formation of new barrier potentials which when subjected to ac fields display overall increase in macroscopic conductivity and also manifest itself in terms of observed multiple dielectric relaxations in modulus study.

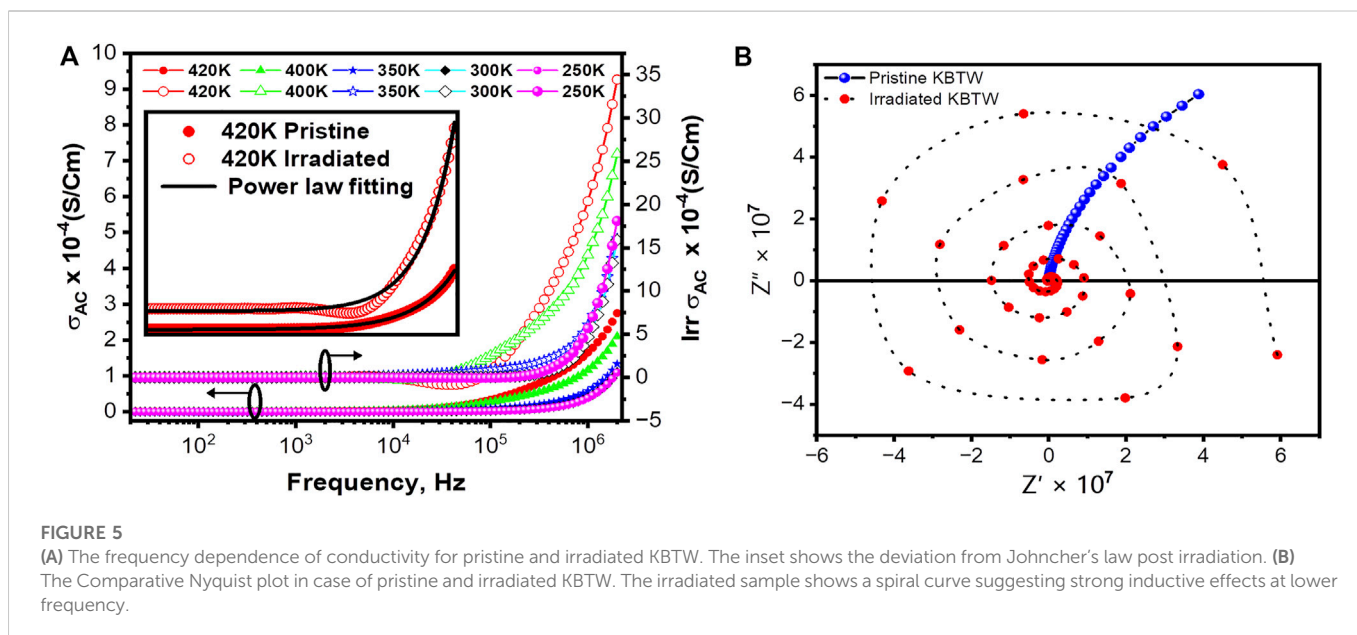


FIGURE 5

(A) The frequency dependence of conductivity for pristine and irradiated KBTW. The inset shows the deviation from Jonscher's law post irradiation. (B) The Comparative Nyquist plot in case of pristine and irradiated KBTW. The irradiated sample shows a spiral curve suggesting strong inductive effects at lower frequency.

**Nyquist Plot analysis:** The Nyquist representation in complex impedance plane for pristine and irradiated Aurivillius at 400 K is shown in Figure 5B. The pristine sample shows a portion of semi-circle which can further modeled to calculate the impedance contribution by grain and grain boundaries. In present case this circuit can be seen as combination of one parallel R-C circuit in series with R. This R and R-C represents the grain and grain boundary contributions respectively. However, the electro-chemical impedance for irradiated sample exhibits an unconventional spiral curve. The divergence from true semicircle is reported in many complex systems [60, 61]; but the observation of the helical Nyquist plot is a rare phenomenon. A similar curve is observed in impedance analysis of electrodes in Lithium-ion batteries and is termed as inductive loop [62]. This behavior is usually attributed to the solid-electrolyte interphase and a constant phase element is introduced to understand this behavior [63]. As seen in electron micro-graph, the irradiation has fragmented the grains and distorted the grain boundaries due to high energy transfer. Although not completely understood the combinations of various effects (both surface and bulk) could be responsible for the observed inductive behaviour.

### 3.3 Discussion

Materials with negative dielectric constant, although allowed by principle of electrodynamics, are not found in nature. Same is true for dielectric materials, the only counterpart of magnetic phenomena which is missing in the electric order. Nevertheless, these systems have been pursued by the scientific community for long as they exhibit a variety of unusual properties which could revolutionize the existing electronic and photonic technologies. In search of such systems, the first breakthrough was achieved in an artificial structure consisting of a periodic array of copper (non-magnetic) resonators [7]. The interaction of such a composite system with oscillating fields is observed to be analogous to that of neutral plasma. And below the plasma frequency (microwave regime) the system exhibits negative indices. The negative relative permittivity was also observed in Perovskite  $PrMnO_3$ , urea-coated nano-particles, insulating polymers, Modified Rh800 dye, and

array of gold nano-rods [56]; [64-66]. In present work the effective dielectric constant was observed to achieve negative values for the irradiated  $K_2Bi_4Ti_4WO_{18}$  above 350 K. In addition the sample exhibits some unique features such as: the helical Nyquist plot, and multiple dipole relaxations. The seven fold rise in conductivity shows an increase in charge carriers due to impingement of  $Ni^{+11}$  in the insulating matrix of ceramic. This anomalous response observed in bulk properties is clearly due to interplay of many complex dipolar mechanisms. The SHI distorts the homogeneity of the ceramic and is capable of creating defects, charge carriers, dipoles, and shows a plasma like surface effect. As the temperature reaches above a critical value a transition to negative dielectric phase is observed plausibly due to activation of these dipoles.

## 4 Conclusion

In conclusion, the phase pure KBTW was prepared by solid state reaction technique. The structural study shows the formation of SHI induced amorphous structure by disintegration of crystallites and introduction of defects. The irradiated complex oxide shows an anomalous dielectric response such as: deviation of conductivity from Jonscher's behaviour, a helical Nyquist plot and transition to negative dielectric constant state above 350 K. The ceramic is modified post irradiation due to absorption of kinetic energy of ion both *via* electronic and nuclear interactions. These interactions along with impingement of ions create defects, imperfections, and charge separation with modified energy barrier configuration. These dipoles when subjected to external field result in an unconventional macroscopic dielectric response. The phase transition to a phase with negative dielectric constant is attributed to the thermal-induced de-trapping of dipoles.

## Data availability statement

The original contributions presented in the study are included in the article/supplementary material, further inquiries can be directed to the corresponding author.

## Author contributions

RN and SR conceived the work while VS and AK carried out all the experimental work including synthesis of samples. IS helped in design or work and experimental support. RM and SK has provided dielectric and XRD characterization. VK, RN, and SR wrote the manuscript. All authors have discussed all results and the manuscript.

## Funding

One author (SSR) acknowledges the financial support of Science and Engineering Research Board, India (ECR/2017/002691).

## Acknowledgments

The authors acknowledge the Science and Engineering Research Board (SERB), Govt. of India for financial support under sanctioned project no. ECR/2017/002691. The authors also acknowledge the

## References

- Maxwell JC. *Viii. a dynamical theory of the electromagnetic field*. United Kingdom: Philosophical transactions of the Royal Society of London (1865).
- Griffiths DJ. *Introduction to electrodynamics*. 4 edn. Cambridge: Cambridge University Press (2017). doi:10.1017/9781108333511
- Rees WG. *Interaction of electromagnetic radiation with matter*. Cambridge, United Kingdom: Cambridge University Press (2001). doi:10.1017/CBO9780511812903.004
- Kao KC. 1 - introduction. In: KC Kao, editor. *Dielectric phenomena in solids*. San Diego: Academic Press (2004). p. 1–39. doi:10.1016/B978-012396561-5/50011-6
- Kao KC. 2 - electric polarization and relaxation. In: KC Kao, editor. *Dielectric phenomena in solids*. San Diego: Academic Press (2004). p. 41–114. doi:10.1016/B978-012396561-5/50012-8
- Viktor GV. The electrodynamic of substances with simultaneously negative values of  $\epsilon$  and  $m$ . *Soviet Phys Uspekhi* (1968) 10:509–14.
- Porto J, Garcia-Vidal F, Pendry J. Transmission resonances on metallic gratings with very narrow slits. *Phys Rev Lett* (1999) 83:2845–8. doi:10.1103/physrevlett.83.2845
- Smith DR, Padilla WJ, Vier D, Nemat-Nasser SC, Schultz S. Composite medium with simultaneously negative permeability and permittivity. *Phys Rev Lett* (2000) 84:4184–7. doi:10.1103/physrevlett.84.4184
- Shelby RA, Smith DR, Schultz S. Experimental verification of a negative index of refraction. *Science* (2001) 292:77–9. doi:10.1126/science.1058847
- Smith DR, Padilla WJ, Vier DC, Nemat-Nasser SC, Schultz S. Composite medium with simultaneously negative permeability and permittivity. *Phys Rev Lett* (2000) 84:4184–7. doi:10.1103/PhysRevLett.84.4184
- Wei H, Wang H, Xia Y, Cui D, Shi Y, Dong M, et al. An overview of lead-free piezoelectric materials and devices. *J Mater Chem C* (2018) 6:12446–67. doi:10.1039/C8TC04515A
- Hussain F, Khesro A, Lu Z, Wang G, Wang D. Lead free multilayer piezoelectric actuators by economically new approach. *Front Mater* (2020) 7. doi:10.3389/fmats.2020.00087
- Maurya D, Peddigari M, Kang M-G, Geng LD, Sharpes N, Annapureddy V, et al. Lead-free piezoelectric materials and composites for high power density energy harvesting. *J Mater Res* (2018) 33:2235–63. doi:10.1557/jmr.2018.172
- Do N-B, Lee H-B, Yoon C-H, Kang J-K, Lee J-S, Kim I-W. Effect of a-t substitution on the ferroelectric and piezoelectric properties of bi 0.5/(na 0.82 k 0.18) 0.5 tio 3 ceramics. *Trans Electr Electron Mater* (2011) 12:64–7. doi:10.4313/teem.2011.12.2.64
- Wu J. Perovskite lead-free piezoelectric ceramics. *J Appl Phys* (2020) 127:190901. doi:10.1063/5.0006261
- Takenaka T, Komura KKK, Sakata KSK. Possibility of new mixed bismuth layered-ferroelectrics. *Jpn J Appl Phys* (1996) 35:5080. doi:10.1143/JJAP.35.5080
- Sun H, Wu Y, Xie X, Lu Y, Yao T, Zhong J, et al. Ferroelectric, magnetic, and optical properties of aurivillius compound  $\text{Bi}_2\text{FeTi}_2\text{Co}_2\text{O}_{15}$ . *J Materiomics* (2018) 4:353–9. doi:10.1016/j.jmat.2018.09.005
- Sharma VK, Nathawat R, Rathore SS. Dielectric properties correlation with microstructure in  $\text{aBi}_4\text{Ti}_4\text{O}_{15}$  ( $a = \text{sr, ba}$ ) bismuth layered ferroelectrics. *Mater Adv* (2022) 3:4890–8. doi:10.1039/D2MA00333C
- Sharma VK, Nathawat R, Chakinala N, Chakinala AGG, Rathore SS. Enhanced photocatalytic properties in metal modified bismuth layered ferroelectric ceramics,  $\text{srb}_4\text{ti}_4\text{o}_{15}$ . *SSRN Electron J* (2022) 2022. doi:10.2139/ssrn.4233197
- Bell AJ, Deubzer O. Lead-free piezoelectrics—The environmental and regulatory issues. *MRS Bull* (2018) 43:581–7. doi:10.1557/mrs.2018.154
- Koruzza J, Bell AJ, Frömling T, Webber KG, Wang K, Rödel J. Requirements for the transfer of lead-free piezoceramics into application. *J Materiomics* (2018) 4:13–26. doi:10.1016/j.jmat.2018.02.001
- Zhang J, Xu D, Tong L, Qi H, Zhang D, Wang C. Surface layer and its effect on dielectric properties of sic ceramics. *J Alloys Comp* (2018) 734:16–21. doi:10.1016/j.jallcom.2017.10.218
- Beier CW, Cuevas MA, Brutchey RL. Effect of surface modification on the dielectric properties of  $\text{BaTiO}_3$  nanocrystals. *Langmuir* (2010) 26:5067–71. doi:10.1021/la9035419
- Hirvonen JK, Clayton CR. *Materials modification by ion implantation*. Boston, MA: Springer US (1983). p. 323–83. doi:10.1007/978-1-4613-3733-1\_12
- McHargue CJ. The mechanical properties of ion implanted ceramics—a review. *Defect and Diffusion Forum* (1988) 57:359–80.
- Picraux ST. Ion implantation in metals. *Annu Rev Mater Sci* (1984) 14:335–72. doi:10.1146/annurev.ms.14.080184.002003
- Page T, Bull S. Ion implantation in ceramics. In: *Reference module in materials science and materials engineering*. Amsterdam, Netherlands: Elsevier (2016). doi:10.1016/B978-0-12-803581-8.03725-5
- Clark J, Pollock J. *Ion implantation and fracture toughness of ceramics*. Australia: Fourth Australian conference on nuclear techniques of analysis: Proceedings (1985).
- Popov V. Ion implantation of polymers: Formation of nanoparticulate materials. *Rev Adv Mater Sci* (2012) 30:1–26.
- Loh I, Oliver R, Sioshansi P. Conducting polymers by ion implantation. *Nucl Instr Methods Phys Res Section B: Beam Interactions Mater Atoms* (1988) 34:337–46. doi:10.1016/0168-583x(88)90054-7
- Rautray TR, Narayanan R, Kwon T-Y, Kim K-H. Surface modification of titanium and titanium alloys by ion implantation. *J Biomed Mater Res B: Appl Biomater* (2010) 93: 581–91. doi:10.1002/jbm.b.31596
- Müller-Steinhagen H, Zhao Q. Investigation of low fouling surface alloys made by ion implantation technology. *Chem Eng Sci* (1997) 52:3321–32. doi:10.1016/s0009-2509(97)00162-0
- Höchbauer T, Misra A, Hattar K, Hoagland R. Influence of interfaces on the storage of ion-implanted he in multilayered metallic composites. *J Appl Phys* (2005) 98:123516. doi:10.1063/1.2149168

34. Magruder R, III, Yang L, Haglund R, Jr, White C, Yang L, Dorsinville R, et al. Optical properties of gold nanocluster composites formed by deep ion implantation in silica. *Appl Phys Lett* (1993) 62:1730–2. doi:10.1063/1.109588
35. Madauß L, Ochedowski O, Lebius H, Ban-d'Etat B, Naylor CH, Johnson AC, et al. Defect engineering of single- and few-layer mos<sub>2</sub> by swift heavy ion irradiation. *2D Mater* (2016) 4:015034. doi:10.1088/2053-1583/4/1/015034
36. Zhu Y, Cai Z, Budhani R, Suenaga M, Welch D. Structures and effects of radiation damage in cuprate superconductors irradiated with several-hundred-mev heavy ions. *Phys Rev B* (1993) 48:6436–50. doi:10.1103/physrevb.48.6436
37. Douillard L, Duraud J. Swift heavy ion amorphization of quartz—A comparative study of the particle amorphization mechanism of quartz. *Nucl Instr Methods Phys Res Section B: Beam Interactions Mater Atoms* (1996) 107:212–7. doi:10.1016/0168-583x(95)01044-0
38. Costantini J-M, Beuneu F. Point defects induced in yttria-stabilized zirconia by electron and swift heavy ion irradiations. *J Phys Condensed Matter* (2011) 23:115902. doi:10.1088/0953-8984/23/11/115902
39. Dufour C, Audouard A, Beuneu F, Dural J, Girard J, Hairie A, et al. A high-resistivity phase induced by swift heavy-ion irradiation of bi: A probe for thermal spike damage? *J Phys Condensed Matter* (1993) 5:4573–84. doi:10.1088/0953-8984/5/26/027
40. Singh Solanki R, Patel JP, Rath C, Kulriya PK, Avasthi DK, Pandey D. Swift heavy ion irradiation induced structural phase transitions in batio<sub>3</sub>: An in-situ x-ray diffraction study (2017). *arXiv e-prints arXiv:1703*.
41. Ziegler JF, Ziegler M, Biersack J. Srim – The stopping and range of ions in matter (2010). *Nucl Instr Methods Phys Res Section B: Beam Interactions Mater Atoms* (2010) 268:1818–23. doi:10.1016/j.nimb.2010.02.091
42. Park S, Lang M, Tracy CL, Zhang J, Zhang F, Trautmann C, et al. Swift heavy ion irradiation-induced amorphization of la<sub>2</sub>ti<sub>2</sub>o<sub>7</sub>. *Nucl Instr Methods Phys Res Section B: Beam Interactions Mater Atoms* (2014) 326:145–9. doi:10.1016/j.nimb.2013.10.088
43. Lang M, Zhang F, Li W, Severin D, Bender M, Klaumünzer S, et al. Swift heavy ion-induced amorphization of cazro<sub>3</sub> perovskite. *Nucl Instr Methods Phys Res Section B: Beam Interactions Mater Atoms* (2012) 286:271–6. doi:10.1016/j.nimb.2011.12.028
44. Pandian M, Krishnaprasanth A, Palanisamy M, Bangaru G, Meena R, Dong C-L, et al. Effects of heavy ion irradiation on the thermoelectric properties of in<sub>2</sub> (te<sub>1-x</sub>sex)<sub>3</sub> thin films. *Nanomaterials* (2022) 12:3782. doi:10.3390/nano12213782
45. Sinduja M, Amirthapandian S, Magudapathy P, Masarat A, Krishnan R, Srivastava S, et al. Role of ion irradiation induced defects in thermoelectric transport properties of bi<sub>2</sub>te<sub>3</sub> thin films. *Thin Solid Films* (2021) 734:138830. doi:10.1016/j.tsf.2021.138830
46. Gadani K, Rathod K, Shrimali V, Rajyaguru B, Udeshi B, Vadgama V, et al. Effect of 200 mev ag<sup>+</sup> 15 ion irradiation on structural, microstructural and dielectric properties of y<sub>0</sub>-95sr<sub>0</sub>-05mno<sub>3</sub> manganite films. *Solid State Commun* (2020) 318:113975. doi:10.1016/j.ssc.2020.113975
47. Kalita P, Ghosh S, Gutierrez G, Rajput P, Grover V, Sattonnay G, et al. Grain size effect on the radiation damage tolerance of cubic zirconia against simultaneous low and high energy heavy ions: Nano triumphs bulk. *Scientific Rep* (2021) 11:10886–10. doi:10.1038/s41598-021-90214-6
48. Sharma M, Gaur A, Quamara JK. Effect of 80 mev o<sup>6+</sup> ion irradiation on structural, morphological, dielectric, and ferroelectric properties of (1-x) pvd<sub>f</sub>(x) batio<sub>3</sub> nanocomposites. *Ionics* (2020) 26:471–81. doi:10.1007/s11581-019-03163-6
49. Niu T, Rayaprolu S, Shang Z, Sun T, Fan C, Zhang Y, et al. *In situ* study on heavy ion irradiation induced microstructure evolution in single crystal cu with nanovoids at elevated temperature. *Mater Today Commun* (2022) 33:104418. doi:10.1016/j.mtcomm.2022.104418
50. Salame PH, Prakash O, Kulkarni AR. Colossal dielectric constant and extremely low loss in t-type la<sub>2</sub>cuo<sub>4</sub>- $\delta$  ceramics. *Ceramics Int* (2016) 42:13207–14. doi:10.1016/j.ceramint.2016.05.113
51. Rathore SS, Nathawat R, Vitta S. A 'mixed' dielectric response in langasite ba<sub>3</sub>nbfe<sub>3</sub>si<sub>2</sub>o<sub>14</sub>. *Phys Chem Chem Phys* (2021) 23:554–62. doi:10.1039/d0cp04965d
52. Sharma VK, Nathawat R, Rathore SS. Structural, thermal and dielectric studies of mixed spinel cofe<sub>2</sub>o<sub>4</sub>. *Mater Today Proc* (2021) 46:2193–6. doi:10.1016/j.matpr.2021.03.153
53. Rayssi C, Kossi SE, Dhahri J, Khirouni K. Frequency and temperature-dependence of dielectric permittivity and electric modulus studies of the solid solution Ca<sub>0.85</sub>Er<sub>0.1</sub>Ti<sub>1-x</sub>Co<sub>0.4x</sub>/3O<sub>3</sub> (0 ≤ x ≤ 0.1). *Rsc Adv* (2018) 8:17139–50. doi:10.1039/c8ra00794b
54. Narang SB, Kaur D, Pubby K. Frequency and temperature dependence of dielectric and electric properties of Ba<sub>2-x</sub>Sm<sub>4+2x/3</sub>Ti<sub>8</sub>O<sub>24</sub> with structural analysis. *Mater Science-Poland* (2015) 33:268–77. doi:10.1515/msp-2015-0034
55. Santhosh Kumar T, Pamu D. Temperature dependent dielectric properties of ba (zn<sup>1/3</sup> ta<sup>2/3</sup>) o<sub>3</sub> ceramics. *XVI Natl Semin Ferroelectrics Dielectrics (Nsfid-xvi)* (2011) 1372:20–3.
56. Balu SK, Shanker NP, Manikandan M, Aparnadevi N, Mukilraj T, Manimuthu P, et al. Crossover to negative dielectric constant in perovskite prmo<sub>3</sub>. *physica status solidi (a)* (2020) 217:2000230. doi:10.1002/pssa.202000230
57. Rathore SS, Vitta S. Effect of divalent ba cation substitution with sr on coupled 'multiglass' state in the magnetolectric multiferroic compound ba<sub>3</sub>nbfe<sub>3</sub>si<sub>2</sub>o<sub>14</sub>. *Scientific Rep* (2015) 5:9751–11. doi:10.1038/srep09751
58. Park Y, Knowles KM. Glass-like behaviour in the relaxor ferroelectric 0.6 pb (-0.4 pb). *J Phys D: Appl Phys* (1999) 32:504–12. doi:10.1088/0022-3727/32/4/020
59. Jonscher AK. The 'universal' dielectric response. *nature* (1977) 267:673–9. doi:10.1038/267673a0
60. Magar HS, Hassan RY, Mulchandani A. Electrochemical impedance spectroscopy (eis): Principles, construction, and biosensing applications. *Sensors* (2021) 21:6578. doi:10.3390/s21196578
61. Allison A, Andreas H. Minimizing the nyquist-plot semi-circle of pseudocapacitive manganese oxides through modification of the oxide-substrate interface resistance. *J Power Sourc* (2019) 426:93–6. doi:10.1016/j.jpowsour.2019.04.029
62. Itagaki M, Taya A, Watanabe K, Noda K. Deviations of capacitive and inductive loops in the electrochemical impedance of a dissolving iron electrode. *Anal Sci* (2002) 18:641–4. doi:10.2116/analsci.18.641
63. Jorcín J-B, Orazem ME, Pébère N, Tribollet B. Cpe analysis by local electrochemical impedance spectroscopy. *Electrochimica Acta* (2006) 51:1473–9. doi:10.1016/j.electacta.2005.02.128
64. Yan H, Zhao C, Wang K, Deng L, Ma M, Xu G. Negative dielectric constant manifested by static electricity. *Appl Phys Lett* (2013) 102:062904. doi:10.1063/1.4792064
65. Shalaev VM, Cai W, Chettiar UK, Yuan H-K, Sarychev AK, Drachev VP, et al. Negative index of refraction in optical metamaterials. *Opt Lett* (2005) 30:3356–8. doi:10.1364/OL.30.003356
66. Shulman J, Tsui S, Chen F, Xue Y, Chu CW. Negative static dielectric constant in a nano-colloid. In: APS Meeting Abstracts; March 13–17, 2006; Baltimore (2006).